Physics of Fluids

Manuscript for *Physics of Fluid*s

Nonequilibrium Molecular Dynamics Study on Energy Accommodation Coefficient on Condensing Liquid Surface —molecular boundary conditions for heat and mass transfer

Atsushi TOKUNAGA (徳永敦士)[a] **and Takaharu TSURUTA** (鶴田隆治)[b, *]

[a] Department of Mechanical Engineering, National Institute of Technology, Ube College, 2-14-1 Tokiwadai, Ube 755-8555, Japan

[b] Department of Mechanical Engineering, Kyushu Institute of Technology, 1-1 Sensui, Tobata-ku, Kitakyushu 804-8550, Japan

* Corresponding author's E-mail: tsuruta.takaharu393@mail.kyutech.jp

ABSTRACT

Nonequilibrium molecular dynamics (NEMD) studies have been conducted to determine molecular boundary conditions at vapor–liquid interfaces for the kinetic theory of condensation and evaporation. In previous studies, a microscopic formulation of the condensation coefficient was defined as the condensation probability of vapor molecules based on equilibrium molecular dynamics simulations and transition state theory. The condensation coefficient was presented as a function of the translation energy of incoming molecules and surface temperature. Based on this, the velocity distributions of evaporating and reflecting molecules were theoretically expressed under equilibrium conditions. In a practical nonequilibrium situation, the energy transfer by the reflecting molecules is important along with the condensation/evaporation probability. However, it is unclear whether the results obtained under equilibrium conditions can be applied under nonequilibrium conditions. This study, therefore, defines the energy accommodation coefficient of reflecting molecules by comparing the energy transfer due to reflection with that under equilibrium conditions. NEMD simulations are conducted using two surfaces facing each other, an evaporating surface and a condensing surface, for argon molecules under different nonequilibrium conditions. The results show that the velocity distribution of reflecting molecules deviates from those under equilibrium conditions, and the energy accommodation coefficient decreases as nonequilibrium conditions increase. Additionally, an inverted temperature profile is observed. Reflecting molecules play an important role in the sensible heat transfer on the condensing surface, and they are not accommodated on the condensing surface. Thus, they raise the temperature in the vicinity of the condensing surface under nonequilibrium conditions.

I. INTRODUCTION

Evaporation and condensation play an important role in heat and mass transfer in thermal science and engineering. In particular, in microscale and nanoscale systems, the interfacial transport resistance at the liquid surface is important because the conductive resistance within a liquid decreases significantly. The kinetic theory of gases is useful in describing the interphase heat and mass transfer between a liquid and a vapor.[1] Based on the Hertz–Knudsen formulation method, the Schrage relationships are widely used for expressing the rate of evaporation and condensation in terms of local interfacial thermodynamics properties.[2] The condensation/evaporation coefficient is an important parameter used to describe the mass flux through a liquid–vapor interface in the expression. In most studies, the condensation coefficient has been considered a constant value of less than or equal to unity without considering the kinetic motion of incident vapor molecules.[3–15] In other words, in those studies, it is assumed that all molecules condense with the same probability, irrespective of their kinetic motion.

However, considering the condensation coefficient as the condensation probability of the incident molecules, it becomes apparent that the condensation coefficient depends on the normal component of the velocity of incident molecules.[16–19] Furthermore, it has been shown that the velocity distributions of evaporating and reflecting molecules in the vicinity of a liquid surface are different from the Maxwellian distribution. Under thermal equilibrium conditions, the Maxwellian distribution can be applied to all leaving molecules but not to evaporating and reflecting molecules. Bond and Struchtrup[20] accepted the molecular velocity-dependent condensation coefficient and indicated the existence of much larger interface temperature jumps, as subsequently observed in experiments by Fang and Ward[21].

The molecular behaviors at a liquid–vapor interface during condensation are classified

into three types—evaporation, condensation, and reflection—as shown in Fig. 1. To express accurately heat and mass transfer, the molecular boundary conditions for these molecules should be based on the kinetic theory of condensation. Numerous recent studies have been conducted based on the Maxwellian distribution, as stated above. In such cases, the kinetic theory may be responsible for a large difference in the temperature profile of a vapor phase. A typical example is an inverted temperature profile that was first reported by Pao[22] in 1971. Since then, numerous works[23–31] have considered this profile as a paradox in thermodynamics from the viewpoint of the second law of thermodynamics because vapor temperature increases as the vapor approaches a condensing surface. It has been concluded that an inverted temperature profile actually exists and does not violate the second law of thermodynamics. However, a clear physical explanation of this profile requires more details on the molecular interaction at the vapor–liquid interfaces, particularly the energy transfer by reflecting molecules. Latent heat transfer can be determined using the net rate of mass transfer obtained from the difference between the condensation and evaporation rates using the condensation/evaporation coefficient or the mass accommodation coefficient. This method is similar to the expression of the Hertz–Knudsen equation and it does not include the sensible heat transfer. As depicted in Fig. 1, the sensible heat transfer by the reflecting vapor molecules without phase change should be considered for a full description of interface heat transfer. In other words, to describe the energy transfer by the vapor molecules reflected at the liquid surface, it is necessary to obtain an energy accommodation coefficient similar to that of a solid surface. Wu and Struchtrup[32] pointed out that the Epstein model[33], which introduced the molecular velocity-dependent accommodation coefficient to the Maxwell model consisting of diffuse and specular reflections, should be used for the boundary condition for molecular reflection on solid surfaces. The present study focuses on both the molecular velocity-dependent

condensation/evaporation coefficient to describe latent heat transfer due to phase change and the molecular velocity-dependent energy accommodation coefficient to describe sensible heat transfer by reflected molecules without phase change. Both of these velocity-dependent coefficients—the condensation/evaporation coefficient and the energy accommodation coefficient—have the possibility to express the molecular velocity distributions properly for the evaporating molecules and the reflecting molecules at the vapor–liquid interface under nonequilibrium conditions.

It was shown that the molecular velocity distributions of evaporating and reflecting molecules can be well modified from the Maxwell distribution by using the velocity-dependent condensation/evaporation coefficient under equilibrium conditions.[16–19] In the present study, nonequilibrium molecular dynamics (NEMD) simulations are carried out to obtain the molecular boundary conditions for the velocity distributions of evaporating and reflecting molecules at a vapor–liquid interface, and the effects of nonequilibrium molecular flow on the velocity distributions examined by comparing those for the equilibrium condition. The simulations are conducted using two surfaces facing each other, i.e., an evaporating surface and a condensing surface, for an argon molecule system under different nonequilibrium conditions. A new definition of the energy accommodation coefficient of reflecting molecules is defined by comparing the energy transfer due to reflection with the energy transfer under equilibrium conditions. In addition, an inverted temperature profile is discussed based on the direct simulation of the Monte Carlo (DSMC) method and application of modified molecular boundary conditions. The condensation coefficient is considered as the condensation probability of incident molecules, and the velocity distribution density of the evaporating molecules and the energy accommodation coefficient of the reflecting molecules are applied. Further, the sensible heat transfer by the reflecting molecules is identified as a key factor for a clear

explanation of the inverted temperature profile at the condensing surface.

II. MOLECULAR BOUNDARY CONDITIONS FOR KINETIC THEORY

The kinetic boundary conditions at the liquid–vapor interfaces require two types of molecular information. One is the condensation probability (i.e., the condensation coefficient) and the other is the velocity distribution functions of the evaporating and reflecting molecules. Typically, the condensation coefficient is assumed to be constant, and the velocity distribution functions are based on the Maxwellian velocity distribution function. However, Tsuruta et al.[16] and Tsuruta and Nagayama[18] found that the condensation coefficient was not an isotropic uniform value but increased with the surface-normal component of the translation energy of incident molecules, as shown in Fig. 2, as per the molecular dynamics (MD) studies of argon and water under thermal equilibrium conditions. An incident molecule with high energy can penetrate more deeply into the vapor–liquid interface region, where it will undergo many interactions with liquid molecules and dissipate energy to the liquid; this increases the condensation probability. A higher surface temperature increases the energy of the surface molecules and thus the likelihood of incident molecules having collisions directly at the surface. This reduces incident molecule penetration, which results in a smaller condensation probability. To express this behavior, the following formulation was introduced by Tsuruta et al.[16] for the first time in the literature:

$$\sigma_c = \alpha\left\{1 - \beta exp\left(-\frac{mV_z^2}{2k_BT}\right)\right\}, \quad (1)$$

where V_z is the component of molecular velocity that is normal to the liquid surface, k_B is the Boltzmann constant, m is the mass of a molecule, and T is the temperature of the liquid surface. Parameters α and β were originally constants for expressing the MD results, but they were defined according to the transition state theory as the functions of the specific

volume of a vapor and liquid, as shown later.[17]

In addition, the velocity distributions of the evaporating and reflecting molecules differed from the Maxwellian distribution in the direction perpendicular to the interface. Under equilibrium conditions, all molecules that leave from a liquid surface should follow the Maxwellian velocity distribution and the evaporation coefficient should be equal to the condensation coefficient because the evaporation and condensation fluxes are the same. Therefore, the velocity distribution functions for the evaporating and reflecting molecules can be modified using Eq. (1) as follows:

$$f_{\mathrm{e,z}} = \sigma_c f_{Maxwellian} = \sigma_c \ \mathrm{n}\left(\frac{m}{2\pi k_B T}\right)^{1/2} exp\left(-\frac{mV_z^2}{2k_B T}\right), \tag{2}$$

$$f_{\mathrm{r,z}} = (1-\sigma_c) f_{Maxwellian} = (1-\sigma_c) \ \mathrm{n}\left(\frac{m}{2\pi k_B T}\right)^{1/2} exp\left(-\frac{mV_z^2}{2k_B T}\right). \tag{3}$$

For the tangential velocity distributions functions, f_x and f_y, it has been reported that there are no marked differences with the Maxwellian distribution.[16, 18]

The number flux of incident molecules is given by the Maxwellian velocity distribution under thermal equilibrium conditions. Thus, the average value of the condensation coefficient, i.e., the macroscopic condensation coefficient can be expressed as follows:

$$\bar{\sigma}_{\mathrm{c}} = \frac{1}{(k_B T/2\pi m)^{1/2}} \int_0^\infty \sigma_c \ V_z \left(\frac{m}{2\pi k_B T}\right)^{1/2} exp\left(-\frac{mV_z^2}{2k_B T}\right) dV_z = \alpha\left(1-\frac{\beta}{2}\right). \tag{4}$$

According to the transition state theory,[17] the average condensation coefficient is formulated as

$$\bar{\sigma}_{\mathrm{c}} = \left(1-\sqrt[3]{V^l/V^g}\right) exp\left(-\frac{1}{2}\frac{1}{\sqrt[3]{V^g/V^l}-1}\right). \tag{5}$$

By comparing Eq. (4) from the MD simulation and Eq. (5) from the transition theory, it is found that two parameters α and β can be obtained as follows:

$$\alpha = exp\left(-\frac{1}{2}\frac{1}{\sqrt[3]{V^g/V^l}-1}\right), \ \beta = 2\sqrt[3]{V^l/V^g}. \tag{6}$$

These relationships can be utilized to predict the condensation coefficient based on the specific volume ratio, $\sqrt[3]{V^l/V^g}$.

The density functions of the velocity distribution, F_r and F_e, are obtained by normalizing Eqs. (2) and (3), respectively, as follows:

$$F_{r,\mathrm{z}} = \frac{1-\alpha+\alpha\beta exp\{-mV_z^2/(2k_BT)\}}{1-\alpha(1-\beta/2)}\left(\frac{m}{k_BT}\right)V_z exp\left(-\frac{mV_z^2}{2k_BT}\right), \quad (7)$$

$$F_{e,\mathrm{z}} = \frac{1-\beta exp\{-mV_z^2/(2k_BT)\}}{1-\beta/2}\left(\frac{m}{k_BT}\right)V_z exp\left(-\frac{mV_z^2}{2k_BT}\right). \quad (8)$$

These formulas have been validated through MD studies.[16-19] Figure 3 shows a comparison of the velocity distribution density functions for the surface-normal component for the evaporating and reflecting molecules and all leaving molecules.[18] It can be observed from the figure that the velocities obtained using Eqs. (7) and (8) are smaller and larger than the Maxwellian velocities, respectively. Hence, the total outgoing molecules (containing the evaporating and reflecting molecules) closely follow the Maxwellian distribution. This implies that the translation energy of evaporating molecules is larger than the average energy described by the Maxwellian distribution. The difference between the energy of the evaporating molecules and the energy based on the Maxwellian distribution is considered to be the energy required to overcome the potential barrier for evaporation. That is, the activation energy can be approximated as follows:

$$\Delta\mathrm{E} = E_{e,\mathrm{z}} - E_{Maxwell,\mathrm{z}} = \int_0^\infty \frac{1}{2}mV_z^2F_{e,z}V_z dV_z - k_BT = \frac{1}{2}\frac{1}{2/\beta-1}k_BT. \quad (9)$$

Therefore, it is understood that Eqs. (1), (7), and (8) can be used as the molecular boundary conditions for the kinetic theory of vapors at an equilibrium liquid surface.

Following these considerations, the DSMC analysis was conducted to examine the inverted temperature profile phenomenon.[19] The resulting temperature profiles are shown in Fig. 4, where the vapor temperature is normalized by the temperature difference ΔT between the bulk vapor and the liquid surface as follows:

$$\theta = \frac{T - T_c}{\Delta T} = \frac{T - T_c}{T_v - T_c}. \tag{10}$$

An inverted temperature profile is observed if an artificial condition, such as perfect condensation ($\sigma_c = 1$, *i.e.*, $\alpha = 1$, $\beta = 0$), is applied as the boundary condition. However, an inverted temperature profile is not observed when Eqs. (1), (7), and (8) are employed, and it is interesting to know that the dimensionless temperature jumps at the interface coincide with each other for the same values of α and β, even under the different supersaturation S, which is defined by Eq. (14) to indicate the nonequilibrium conditions. Therefore, it is generally understood that an inverted temperature profile exists in practical situations. However, the molecular boundary conditions obtained for thermal equilibrium conditions, i.e., Eqs. (1), (7), and (8), cannot express this phenomenon. This shows that nonequilibrium conditions should be included to obtain a full description of heat and mass transfer at the vapor–liquid interfaces.

We assume that molecular evaporation and condensation are characterized mainly by liquid temperature and do not significantly differ under nonequilibrium conditions. This is because evaporation and condensation behaviors depend on the activation energy expressed in Eq. (9). However, it is considered that reflection behavior depends on nonequilibrium conditions. Thus, the energy accommodation coefficient of the reflecting molecules is examined in this study.

III. NEMD SIMULATION METHOD

In this study, NEMD simulations were carried out in a rectangular simulation cell with Lx = Ly = 6.486 nm and Lz = 131.347 nm, where Lx, Ly, and Lz are the length sizes of the simulation cell in the x-, y-, and z-axis directions, respectively, as shown in Fig. 5. The length of the simulation cell in the z direction (flow direction of the vapor) was 30 times the mean free path of argon gas at 100 K. Periodic boundary conditions were applied in the

x, y, and z directions. The total number of particles in the system was 12000, and the cell index method was used to improve the efficiency of the calculation of the force or potential field. The Lennard–Jones potential function was applied to the force field of argon as follows:

$$\Phi_{ij}(r_{ij}) = 4\varepsilon\left\{\left(\frac{\sigma}{r_{ij}}\right)^{12} - \left(\frac{\sigma}{r_{ij}}\right)^{6}\right\}, \tag{11}$$

where ϕ_{ij} is the potential energy between particles i and j at intermolecular distance r_{ij}, σ = 0.3405 nm is the diameter of argon, and ε is the potential parameter of ε/k_B = 119.8 K. The velocity Verlet algorithm was used with a time step of Δt = 5 fs, and the cutoff distance was set to 3.5 σ.

Two thermostats at different temperatures were employed to maintain nonequilibrium conditions. A hot slab and a cold slab were set in the liquid close to the left and right sides of the simulation cell, respectively. The thickness of the thermostat layer was 3.5 σ. Cold liquid temperatures were set to 90 K and 100 K, and hot liquid temperatures were changed such that they were higher than the cold liquid temperatures. Evaporation occurred on the left side, and vapor molecules condensed on the right side. The cell was divided into 110 layers for the local data sampling of temperature and density. It was necessary to distinguish the reflecting molecules from the evaporating molecules. We considered a cutoff time of 20 ps to deduce reflection or evaporation, which corresponded to the interaction time shown in Fig. 1. In particular, an incident molecule was considered to be a reflecting molecule if it returned to the vapor phase within 20 ps. [16-18]

IV. RESULTS AND DISCUSSION

Temperature profiles

The typical temperature profiles obtained by conducting NEMD simulations under different temperature conditions are presented in Fig. 6. The temperatures of the evaporating liquid surface change from 120 K to 130 K, and the temperatures of the condensing liquid surface are maintained at 90 K or 100 K. Thermostat-layer temperatures T^H and T^L are indicated in each figure by solid red and blue circles, respectively. It is understood in these figures that the effects of the thermostat layer are limited within adjacent layers judging from the temperature movement moving up, then down near each thermostat. The liquid surface temperature T^l and the vapor temperature T^{lv} adjacent to the condensation interface are obtained by considering the density profiles along the z direction. The vapor phase temperature T^v is almost uniform except for the regions near the condensation and evaporation interfaces, which indicates that the present simulation cell has sufficient length and molecular number for the steady-state nonequilibrium simulations. Temperature jumps are observed on the evaporating and condensing surfaces, and negative temperature gradients are found in the vicinity of the condensing surface. For instance, in Fig. 6 (d), the vapor temperature at the interface is 4.8 K higher than the bulk phase temperature, T^v = 105.0 K, when the temperatures of the evaporating and condensing surfaces are 130 K and 100 K, respectively. The next subsection further elaborates the temperature changes based on the velocity distributions close to the condensing surface.

Velocity distributions

Here, we discuss the reason for the occurrence of an inverted temperature profile. Figure 7 shows the velocity distributions of vapor molecules in the vicinity of the condensing surface when the temperatures of the evaporating and condensing surfaces are (a) 125 K and 90 K, respectively, and (b) 130 K and 100 K, respectively. The velocity distributions of the evaporating and reflecting molecules are depicted along with those of all leaving molecules.

The velocity distribution of all leaving molecules agrees with the Maxwellian distribution. Moreover, the velocity distribution of the evaporating molecules agrees with the distribution obtained using Eq. (8) under equilibrium conditions. This supports our assumption that evaporation can be represented by the equilibrium relation even under nonequilibrium conditions. However, the velocity distribution of the reflecting molecules is different from the distribution obtained using Eq. (7). The values obtained through NEMD simulation are smaller than those obtained using Eq. (7) in the low-velocity region (at approximately 100 m/s) and larger in the high-velocity region (at 300 m/s). This indicates that the energy of the reflecting molecules is larger than the energy under equilibrium conditions. Under nonequilibrium conditions, the reflecting molecules are not accommodated on the liquid surface, that is, the reflection is nonaccommodative. Thus, the reflecting molecules have excess energy under nonequilibrium conditions. It is considered that the energy transfer to the liquid surface is limited, and the excess energy returns to the vapor phase. Therefore, the vapor temperature close to the condensing surface shows a negative gradient.

Energy accommodation coefficient for reflecting molecules

Instead of the conventional accommodation coefficient, a new definition of the energy accommodation coefficient, γ, is proposed for the reflecting molecules as follows:

$$\gamma = \frac{E_i - E_r}{E_i - E_s}, \tag{12}$$

where E_i is the incident energy of reflecting molecules and E_r is the escape energy after reflection. E_s is the energy of the reflecting molecules that are completely accommodated on the liquid surface, and it is obtained using Eq. (7) as follows:

$$E_s = \int_0^\infty \frac{1}{2} m v_z^2 F_{z,r} dv_z = \frac{1-\alpha+\alpha\beta/4}{1-\alpha+\alpha\beta/2} k_B T. \tag{13}$$

In numerous studies, E_s has been obtained based on the Maxwellian distribution. However, the energy of reflecting molecules is lower than that obtained using the Maxwellian distribution, as

explained in Section II. Therefore, in the present study, E_s is defined as the energy of the reflecting molecules under equilibrium conditions based on Eq. (7). According to this definition, the energy accommodation coefficient γ is unity for the reflecting molecules under equilibrium conditions. Table I summarizes the energy of the reflecting molecules under equilibrium conditions at different temperatures. For the condensing surface at 100 K, the value of E_s is evaluated to be $0.679k_BT$ (α = 0.923 and β = 0.299), which is smaller than the value of k_BT for the Maxwellian distribution.

Table I Energy of reflecting molecules under equilibrium conditions.

T [K]	α	β	$\frac{E_s}{k_BT}$
90	0.935	0.222	0.694
100	0.923	0.299	0.679
120	0.750	0.388	0.816

The accommodation coefficient obtained by conducting the NEMD simulations is a function of supersaturation S, as shown in Fig. 8, which is defined as the ratio between the pressures of the vapor and liquid surfaces:

$$S = \frac{p_v}{p_c}, \tag{14}$$

where p_v is the pressure of the bulk vapor phase and p_c is the saturation pressure at surface temperature. As supersaturation represents nonequilibrium conditions, the accommodation coefficient is close to unity at a small supersaturation, as shown in Fig. 8. The accommodation coefficient decreases as supersaturation increases, which corresponds to the increasing nonequilibrium conditions. This indicates that the energy of the reflecting molecules is larger than the energy of the reflecting molecules in equilibrium, and

reflecting molecules cannot be accommodated on the condensing liquid surface under nonequilibrium conditions.

Figure 9 shows the velocity distributions of the reflecting molecules on the condensing surface at 100 K. As shown in Fig. 7, under the nonequilibrium condition, the velocity distribution of the reflecting molecules differs from the theoretical equilibrium distribution given by Eq. (7). This difference can be clearly observed in Fig. 9 (a) that shows the velocity distribution of only reflecting molecules. These molecules are classified into three groups depending on the number of interactions with surface molecules in the interface zone, and the velocity distributions of these groups are presented in Fig. 9 (b). The velocity distribution of the reflecting molecules that have a large number of interactions deviates significantly from the theoretical distribution. In contrast, the velocity distribution of the reflecting molecules with less than 10 interactions is close to the theoretical equilibrium distribution. In other words, the velocity distribution of the reflecting molecules approaches that of the evaporating molecules (Eq. (8)) through repeated collisions with the surface molecules. This results in a large energy reflection and decrease in the heat transfer to the liquid surface. Therefore, the energy accommodation coefficient of the reflecting molecules expressed in Eq. (12) decreases as the number of collisions with the surface molecules increases.

Figure 10 presents the vertical (z-direction) location where reflection occurs owing to the final interaction of incident molecules within the interface region. The molecules with fewer than 10 interactions are reflected at a shallow depth at the interface, whereas the molecules with more than 11 interactions are reflected close to the deeper liquid phase. The deeper part of the vapor–liquid interface region has a larger molecular density and a higher chance of collision with molecules compared to the shallow part, as shown in Fig. 10. As the nonequilibrium conditions increase, the number of incident molecules with

higher velocity increases, and these molecules can penetrate the deeper interface region. On this basis, it is understood that the reflecting molecules play an important role in nonequilibrium condensing flow. Therefore, the energy transfer due to the reflecting molecules must be fully analyzed by introducing the velocity-dependent energy accommodation coefficient for nonequilibrium heat transfer.

DSMC analysis

The DSMC analysis is widely used as the solver of the Boltzmann equation with phase change.[34] Its noise-free deterministic method is considered to be much more efficient than the MD simulations. In the present study, the DSMC analysis is performed, and the results are compared to the NEMD simulation results to verify the effect of energy transfer by the reflecting molecules on the inverted temperature profile. The simulation system is shown in Fig. 11. The one-dimensional condensing flow of argon vapor is considered. The bulk vapor phase is separated from the liquid surface by a distance of 30 times the mean free path of argon gas at 100 K. The simulation domain is divided into 90 cells, and the number of sample molecules in a cell is approximately 1,000. The condensing surface temperature is set to 100 K, which is the same as that for the NEMD simulations. The rigid sphere model and maximum collision-number scheme are used for the collisions between particles. The time increment is approximately 10 times smaller than the mean free time, and a simulation period of 100,000 steps is considered to obtain time-averaged results. At the interface, it is determined whether an incident molecule is condensed or reflected based on the condensation coefficient expressed in Eq. (1). The velocity of reflecting molecules is modified through the utilization of the energy accommodation coefficient, as shown in Fig. 8.

The comparison of the temperature profiles, obtained by conducting the DSMC analysis and NEMD simulations, is presented in Fig. 12 in a similar manner to Fig. 4. The dimensionless temperature is defined by Eq. (10). In both cases, temperature close to the condensing surface increases, resulting in an inverted temperature gradient in the vapor phase. The results of the NEMD simulation include a few fluctuations. However, the results of the DSMC analysis present a continuous temperature profile because the DSMC method is a stochastic method. This indicates that the DSMC method with the molecular boundary conditions is useful to understand the condensing flow of molecules.

Figure 13 compares the velocity distributions obtained by conducting NEMD simulations and DSMC analysis; a good agreement is observed between the results. The velocity distribution of the reflecting molecules obtained by conducting the DSMC analysis deviates from the equilibrium distribution obtained using Eq. (7) and agrees with the results of the NEMD simulation, and it shifts to the high-velocity region. This implies that the inverted temperature profile occurs because of the excess energy of the reflecting molecules. Therefore, the present molecular boundary conditions, including the energy accommodation coefficient, are appropriate to predict the heat and mass transfer characteristics on a liquid surface under nonequilibrium conditions.

V. CONCLUSIONS

In this study, NEMD simulations were carried out using argon molecules to formulate the boundary conditions on a condensing liquid surface under nonequilibrium conditions. A new definition of the energy accommodation coefficient of reflecting molecules was introduced by comparing the energy transfer by the reflecting molecules and the energy transfer in equilibrium conditions. The following conclusions were obtained:

1. Under practical nonequilibrium conditions, the sensible heat transfer by the reflecting molecules is important in addition to the latent heat transfer owing to the mass transfer across the vapor–liquid interface. The latent heat transfer can be obtained using the net condensation rate that is defined as the difference between the condensation and evaporation rates using the condensation or evaporation coefficient. For a sensible heat transfer, it is necessary to obtain the energy accommodation coefficient of the reflecting molecules in a manner similar to the heat transfer on a solid surface.
2. The velocity distribution of reflecting molecules deviates from the theoretical distribution in equilibrium conditions to high-velocity regions. In addition, the energy accommodation coefficient of the reflecting molecules decreases as the nonequilibrium conditions increase with a temperature difference between the vapor and liquid surface. This indicates that the energy of the reflecting molecules is larger than the energy under equilibrium conditions. The sensible heat transfer decreases with the accommodation coefficient, i.e., the energy transfer to the liquid surface is limited, and excess energy returns to the vapor phase. This increases the accumulation of excess energy on the liquid surface, which is considered the reason for the occurrence of inverted temperature profiles.
3. The results of the DSMC analysis and NEMD simulations agree if appropriate molecular boundary conditions, such as the velocity distributions of the evaporating and reflecting molecules, are applied along with the condensation coefficient as the condensation probability.

ACKNOWLEDGMENTS

We would like to thank Editage (www.editage.com) for English language editing.

DATA AVAILABILITY

The data that support the findings of this study are available from the corresponding author upon reasonable request.

REFERENCES

1. A. Frezzotti and P. Barbante, "Kinetic theory aspects of non-equilibrium liquid-vapor flows," Mechanical Engineering Reviews. 4, 16 (2017).
2. R. W. Schrage, *A Theoretical Study of Interphase Mass Transfer* (Columbia University Press, New York, 1953).
3. J. Yu and H. Wang, "A molecular dynamics investigation on evaporation of thin liquid films," Int. J. Heat Mass Transf. 55, 1218–1225 (2012).
4. R. E. H. Miles, J. P. Reid, and I. Riipinen, "Comparison of approaches for measuring the mass accommodation coefficient for the condensation of water and sensitivities to uncertainties in thermophysical Properties," J. Phys. Chem. A 116, 10810−10825 (2012).
5. T. Ishiyama, S. Fujikawa, T. Kurz, and W. Lauterborn, "Nonequilibrium kinetic boundary condition at the vapor-liquid interface of argon," Phys. Rev. E 88, 042406 (2013).
6. J. Julin, M. Shiraiwa, R. E. H. Miles, J. P. Reid, U. Pöschl, and I. Riipinen, "Mass accommodation of water: Bridging the gap between molecular dynamics

simulations and kinetic condensation models," J. Phys. Chem. A 117, 410–420 (2013).

7. B. Peng, W. He, X. Hao, Y. Chen, and Y. Liu, "Interfacial thermal conductance and thermal accommodation coefficient of evaporating thin liquid films: A molecular dynamics study," Comput. Mater. Sci. 87, 260–266 (2014).
8. M. Kon, K. Kobayashi, and M. Watanabe, "Method of determining kinetic boundary conditions in net evaporation/condensation," Phys. Fluids 26, 072003 (2014).
9. K. Kobayashi, K. Hori, M. Kon, K. Sasaki, and M. Watanabe, "Molecular dynamics study on evaporation and reflection of monatomic molecules to construct kinetic boundary condition in vapor–liquid equilibria," Heat Mass Transf. 52, 1851–1859 (2016).
10. M. Kon, K. Kobayashi, and M. Watanabe, "Kinetic boundary condition in vapor–liquid two-phase system during unsteady net evaporation/condensation," Eur. J. Mech. B Fluids 64, 81–92 (2017).
11. K. Kobayashi, K. Sasaki, M. Kon, H. Fujii, and M. Watanabe, "Kinetic boundary conditions for vapor–gas binary mixture," Microfluid. Nanofluid. 21, 53 (2017).

12. Z. Liang, T. Biben, and P. Keblinski, "Molecular simulation of steady-state evaporation and condensation: Validity of the Schrage relationships," Int. J. Heat Mass Transf. 114, 105–114 (2017).
13. E. Bird and Z. Liang, "Transport phenomena in the Knudsen layer near an evaporating surface," Phys Rev E 100, 043108 (2019).
14. K. Ohashi, K. Kobayashi, H. Fujii, and M. Watanabe, "Evaporation coefficient and condensation coefficient of vapor under high gas pressure conditions," Sci. Rep. 10, 8143 (2020).
15. K. Montazeri, S. Hao, M. J. Abdolhosseini Qomi, and Y. Won, "Molecular dynamics investigation of liquid and vapor interactions near an evaporating interface: A theoretical genetics perspective," Advanced Theory and Simulations 3, (2020).
16. T. Tsuruta, H. Tanaka, and T. Masuoka, "Condensation/evaporation coefficient and velocity distributions at liquid-vapor interface," Int. J. Heat Mass Transfer. 42 (22), 4107–4116 (1999).
17. G. Nagayama and T. Tsuruta, "A general expression for the condensation coefficient based on transition state theory and molecular dynamics simulation," J. Chem. Phys. 118 (3), 1392–1399 (2003).

18. T. Tsuruta and G. Nagayama, "Molecular dynamics studies on the condensation coefficient of water," J. Phys. Chem. B. 108 (5), 1736–1743 (2004).
19. T. Tsuruta and G. Nagayama, "A microscopic formulation of condensation coefficient and interface transport phenomena," Energy 30 (6), 795–805 (2005).
20. M. Bond and H. Struchtrup, "Mean evaporation and condensation coefficients based on energy dependent condensation probability," Phys. Rev. E Stat. Nonlin. Soft Matter Phys. 70, 061605 (2004).
21. G. Fang and C. A. Ward, "Temperature measured close to the interface of an evaporating liquid," Phys. Rev. E 59, 417–428 (1999).
22. Y. P. Pao, "Application of kinetic theory to the problem of evaporation and condensation," Phys. Fluids 14 (2), 306–312 (1971).
23. L. J. F. Hermans and J. J. M. Beenakker, "The temperature paradox in the kinetic theory of evaporation," Phys. Fluids 29, 4231 (1986).
24. D. Bedeaux, L. J. F. Hermans, and T. Ytrehus, "Slow evaporation and condensation," Physica A 169 (2), 263–280 (1990).
25. T. Ytrehus, "Molecular-flow effects in evaporation and condensation at interface," Multiph. Sci. Technol. 9, 205–327 (1997).

26. S. Kjelstrup, T. Tsuruta, and D. Bedeaux, "The inverted temperature profile across a vapor/liquid surface analyzed by molecular computer simulations," J. Colloid Interface Sci. 256 (2), 451–461 (2002).

27. A. Frezzotti, P. Grosfils, and S. Toxvaerd, "Evidence of an inverted temperature gradient during evaporation/condensation of a Lennard-Jones fluid," Phys. Fluids 15, 2837–2842 (2003).

28. R. Meland, "Molecular dynamics simulation of the inverted temperature gradient phenomenon," Phys. Fluids 15, 3244–3247 (2003).

29. P. N. Shankar and M. D. Deshpande, "On the temperature distribution in liquid–vapor phase change between plane liquid surfaces," Phys Fluids A 2, 1030–1038 (1990).

30. E. Johannessen and D. Bedeaux, "Integral relations for the interfacial heat and mass transfer resistivities and the inverted temperature gradient," Phys. Fluids 19, 017104 (2007).

31. Z. Liang, A. Chandra, E. Bird, and P. Keblinski, "A molecular dynamics study of transient evaporation and condensation," Int. J. Heat Mass Transf. 149, 119152 (2020).

32. L. Wu and H. Struchtrup, "Assessment and development of the gas kinetic boundary condition for the Boltzmann equation," J. Fluid Mech. 823, 511–537 (2017).

33. M. Epstein, "A model of the wall boundary condition in kinetic theory," AIAA Journal 5, 1797–1800 (1967).

34. A. Frezzotti, P. Barbante, and L. Gibelli, "Direct simulation Monte Carlo applications to liquid-vapor flows," Phys. Fluids 31, 062103 (2019).

List of Figure Caption:

Fig. 1 Heat and mass transfer at the vapor–liquid interface.

Fig. 2 Condensation coefficient as condensation probability, which is a function of the normal component of the translational energy of incident molecules[18] (Reproduced with permission from J. Phys. Chem. B. 108-5, 1736 (2004). Copyright 2004 American Chemical Society).

Fig. 3 Velocity distribution density functions for the surface-normal component at the condensing surface of argon under equilibrium conditions at 120 K.[18] (Reproduced with permission from J. Phys. Chem. B. 108-5, 1736 (2004). Copyright 2004 American Chemical Society).

Fig. 4 Comparison of temperature profiles under different boundary conditions at the condensing surface (DSMC results for argon surface at 100 K).[19] The dimensionless temperature θ is based on the overall temperature difference ΔT, and λ is the mean free path. (Reproduced with permission from Energy 30, 795 (2005). Copyright 2005 Elsevier Ltd.).

Fig. 5 NEMD simulation system

Fig. 6 Temperature profiles via NEMD for two cases of the condensing surface temperatures at 90 K ((a), (b)) and 100 K ((c), (d)) under different nonequilibrium conditions. Thermostat-layer temperatures T^H and T^L are indicated by the solid red and blue circles, respectively.

Fig. 7 Velocity distributions obtained via NEMD simulations when the temperatures of the evaporating and condensing surfaces are (a) 125 K and 90 K, respectively, and (b) 130 K and 100 K, respectively.

Fig. 8 Accommodation coefficient of reflecting molecules.

Fig. 9 Velocity distribution of reflecting molecules on the condensing surface at 100 K (T_H=130 K). The velocity distribution (a) shows some shift to the larger velocity region compared to the equilibrium velocity distribution given by Eq. (7). The velocity distribution (b) shows the relation between the interaction number and their velocity distribution density.

(a) Velocity distribution of reflecting molecules only
(b) Classification of reflecting molecules based on number of interactions

Fig. 10 Location of reflection in z direction within the interface region for the case of T^H = 130 K and T^L = 100 K.

Fig. 11 Simulation system and boundary conditions for DSMC analysis.

Fig. 12 Comparison of temperature profiles obtained by conducting NEMD simulations and DSMC analysis.

Fig. 13 Comparison of velocity distributions obtained by conducting NEMD simulations (T^H = 130 K and T^L = 100 K) and DSMC analysis

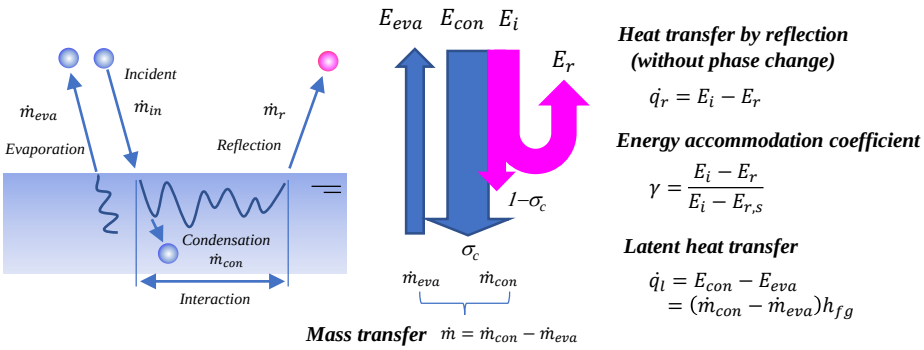

Fig.1 Heat and mass transfer at the vapor-liquid interface.

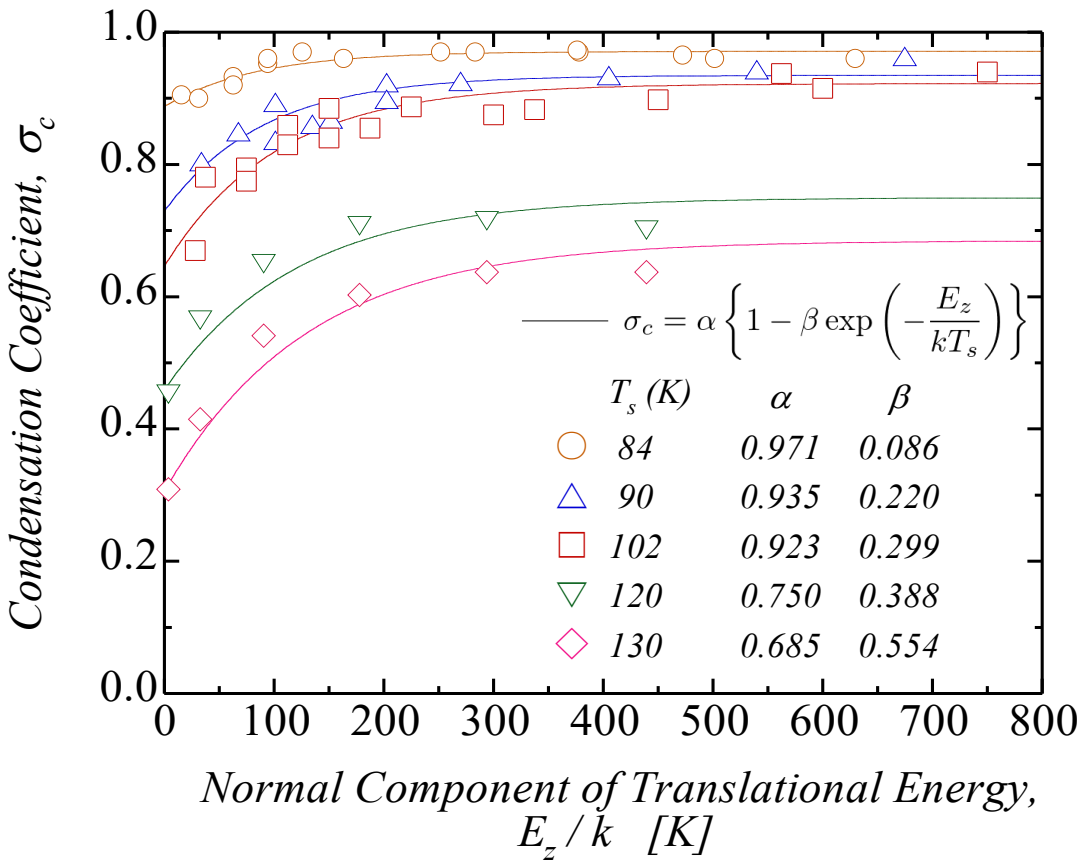

Fig. 2 Condensation coefficient as condensation probability, which is a function of normal component of translational energy of incident molecules[15] (Reproduced with permission from J. Phys. Chem. B. 108-5, 1736 (2004). Copyright 2004 American Chemical Society).

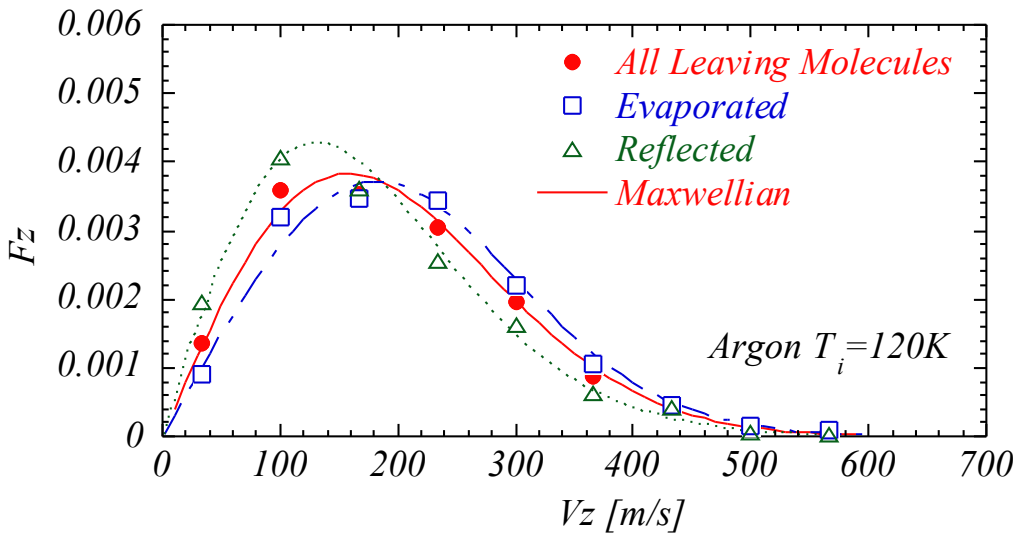

Fig. 3 Velocity distribution density functions for the surface-normal component at the condensing surface of argon under equilibrium conditions at 120 K.[17] (Reproduced with permission from J. Phys. Chem. B. 108-5, 1736 (2004). Copyright 2004 American Chemical Society).

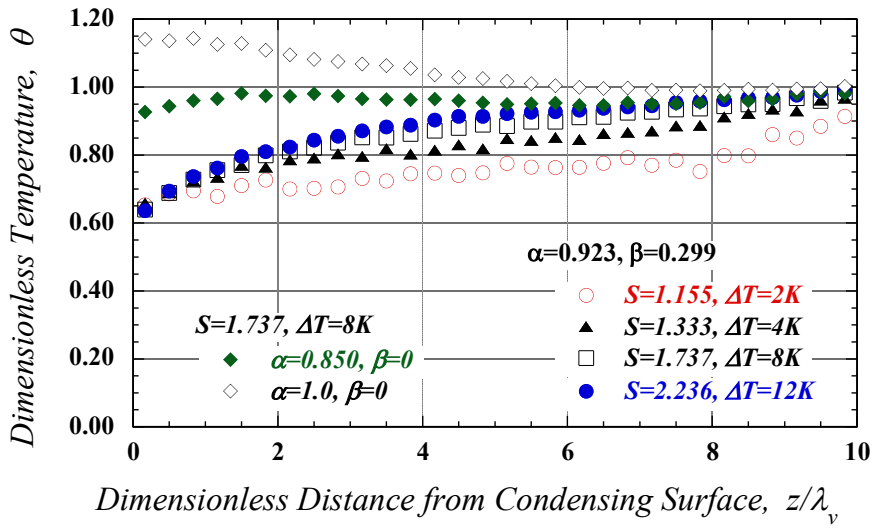

Fig. 4 Comparison of temperature profiles under different boundary conditions at the condensing surface (DSMC results for argon surface at 100 K).[19] The dimensionless temperature θ is based on the overall temperature difference ΔT, and λ is the mean free path. (Reproduced with permission from Energy 30, 795 (2005). Copyright 2005 Elsevier Ltd.).

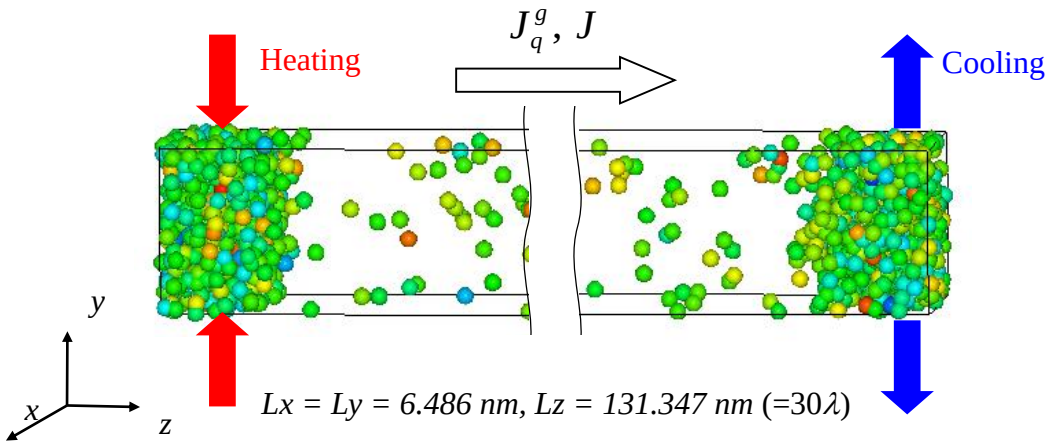

Fig. 5 NEMD simulation system

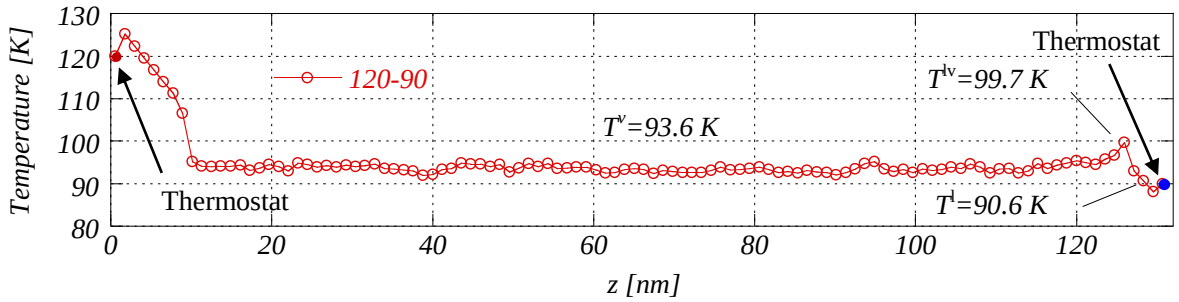

(a) T^H = 120 K, T^L = 90 K

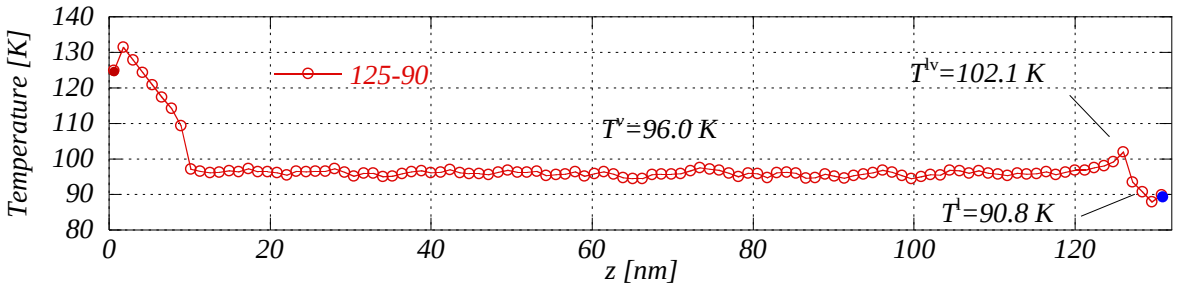

(b) T^H = 125 K, T^L = 90 K

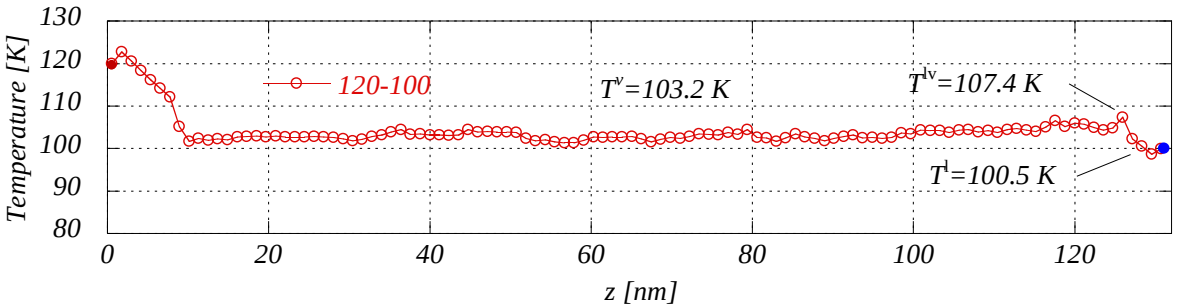

(c) T^H = 120 K, T^L = 100 K

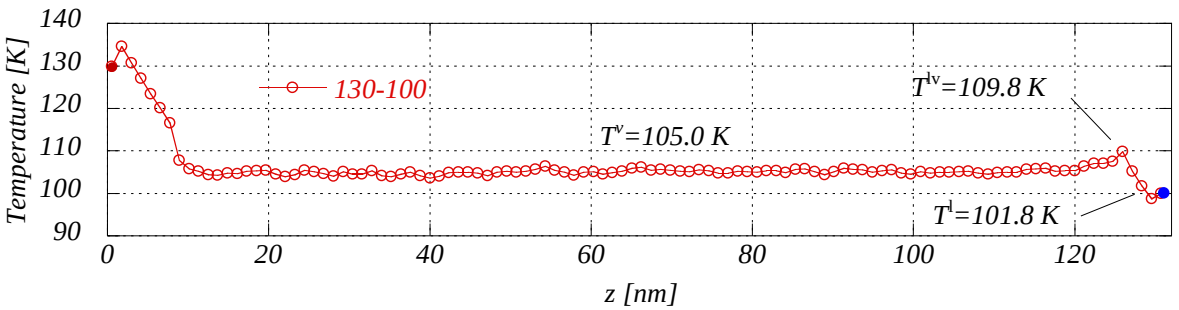

(d) T^H = 130 K, T^L = 100 K

Fig.6 Temperature profiles via NEMD for two cases of the condensing surface temperatures at 90 K ((a), (b)) and 100 K ((c), (d)) under the different nonequilibrium conditions. Thermostat-layer temperatures T^H and T^L are plotted by solid symbols of red and blue, respectively.

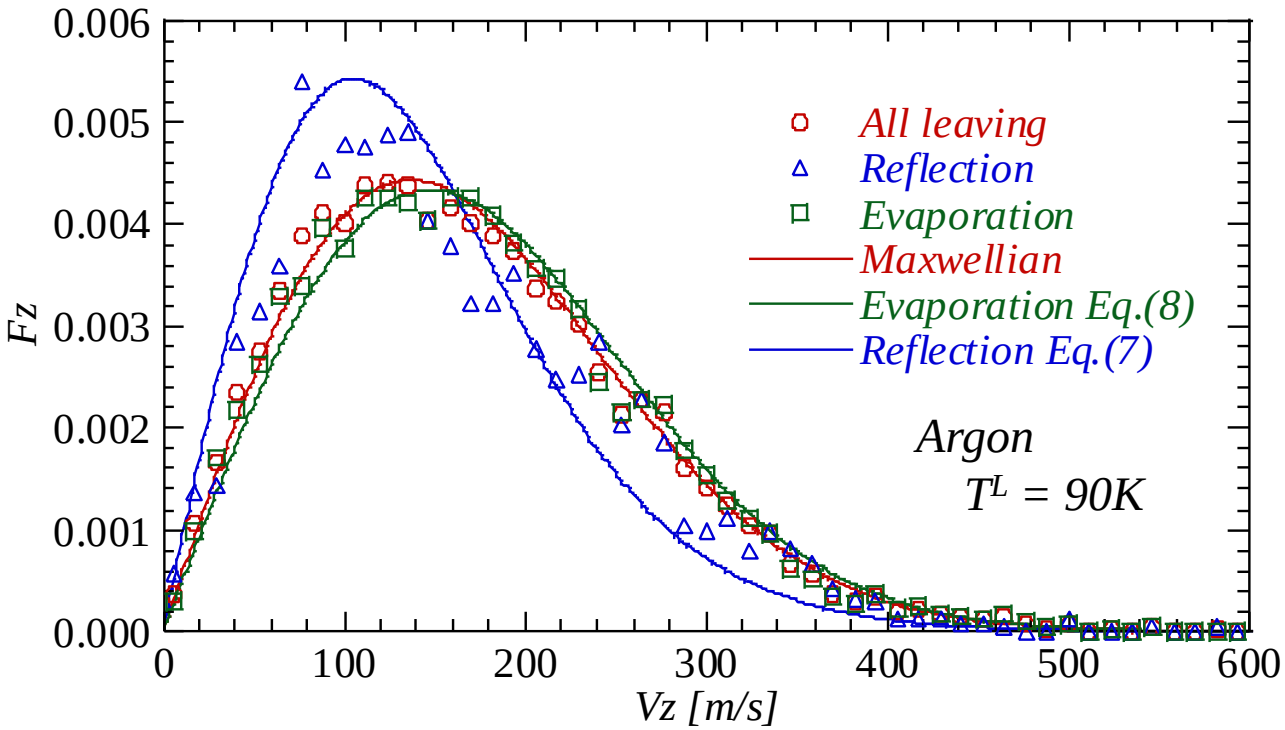

(a) 125 K-90 K

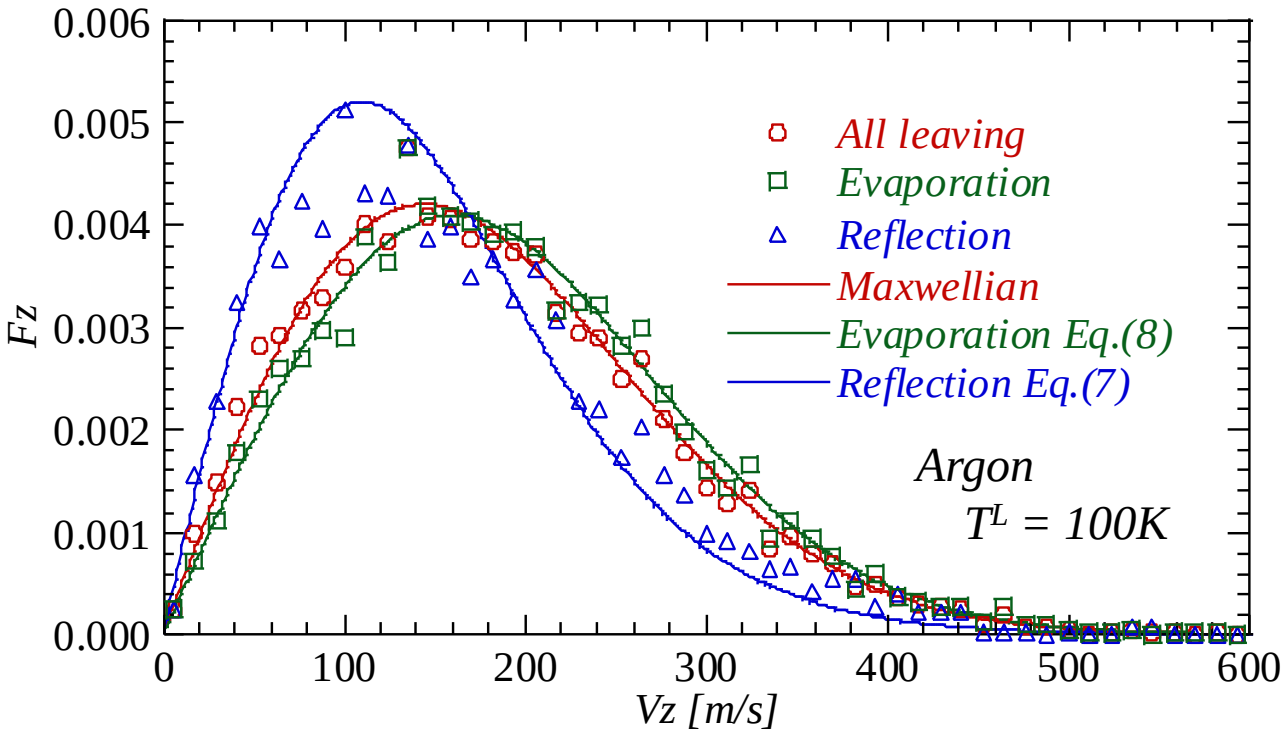

(b) 130 K-100 K

Fig. 7 Velocity distributions obtained via NEMD simulations when temperatures of evaporating and condensing surfaces are (a) 125 K and 90 K, respectively, and (b) 130 K and 100 K, respectively

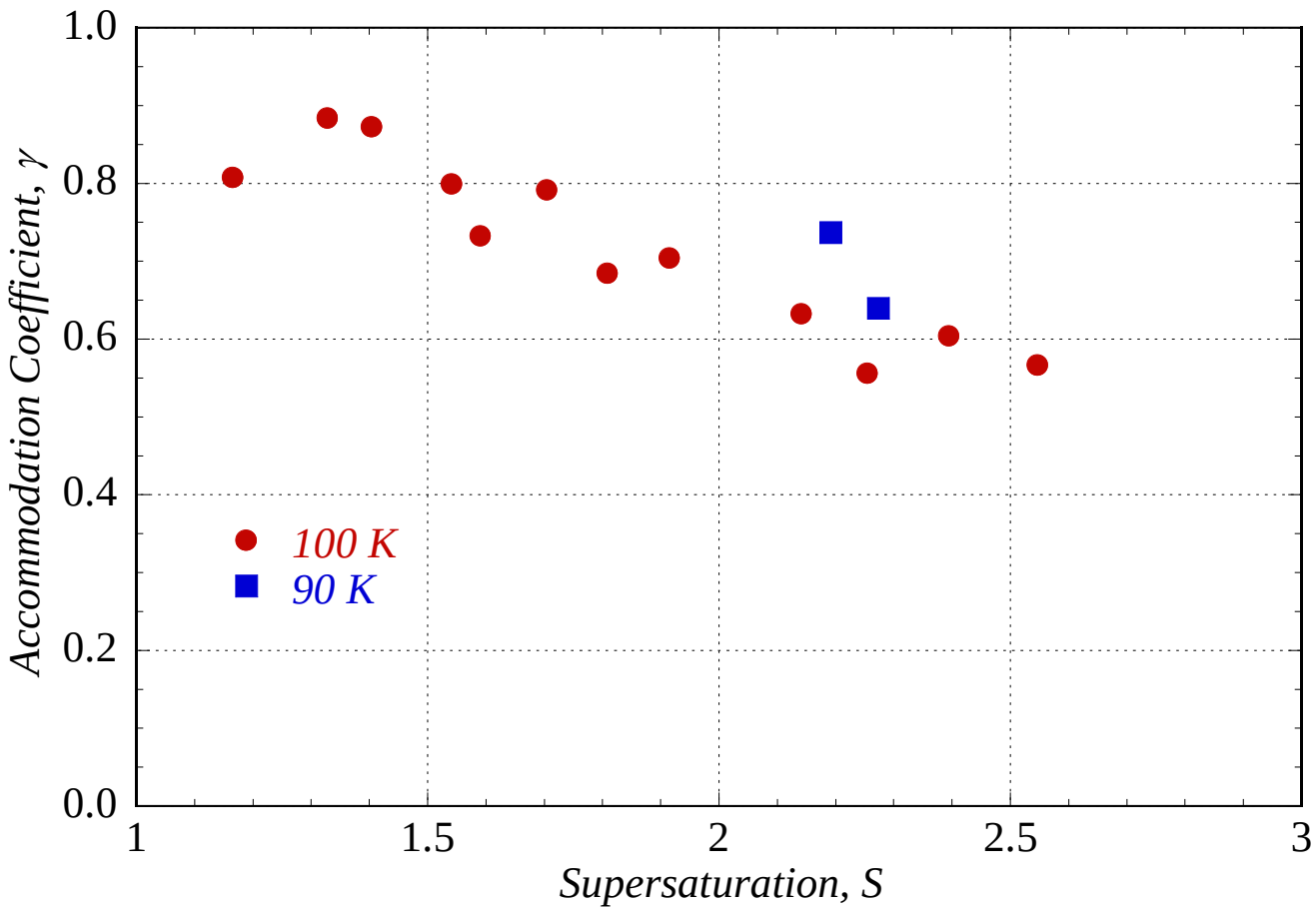

Fig. 8 Accommodation coefficient of reflecting molecules

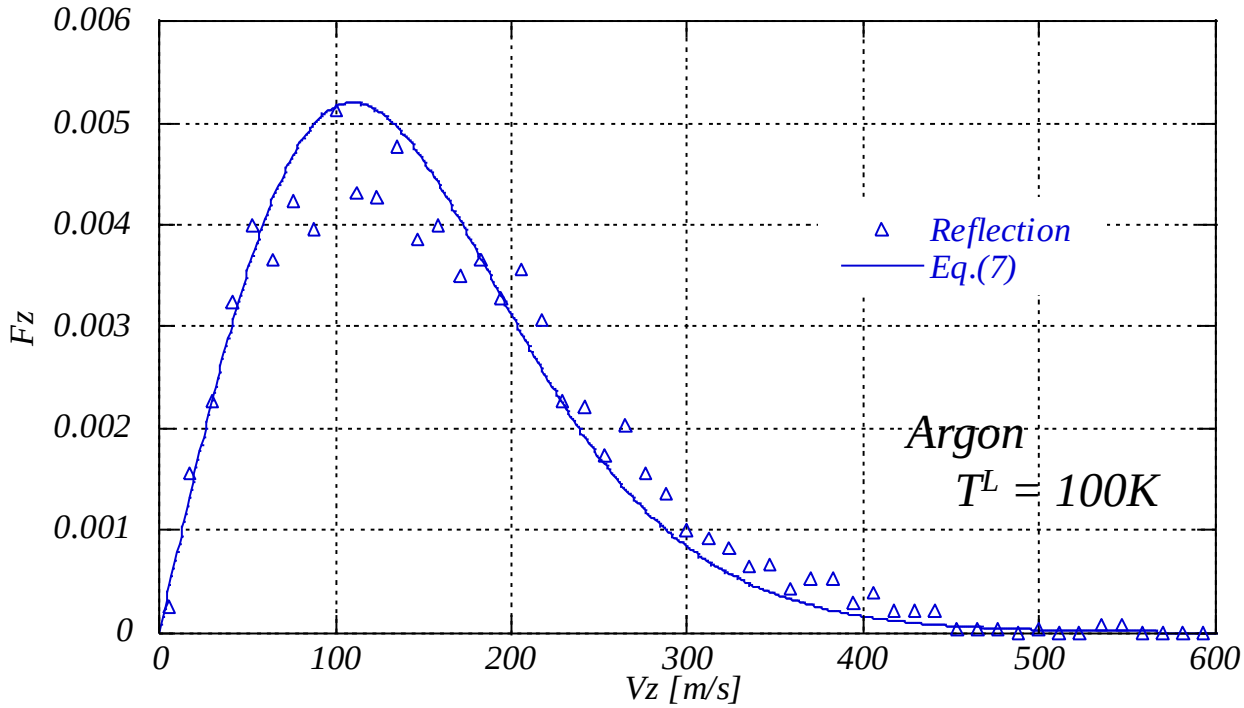

(a) Velocity distribution of only reflecting molecules (130K-100K)

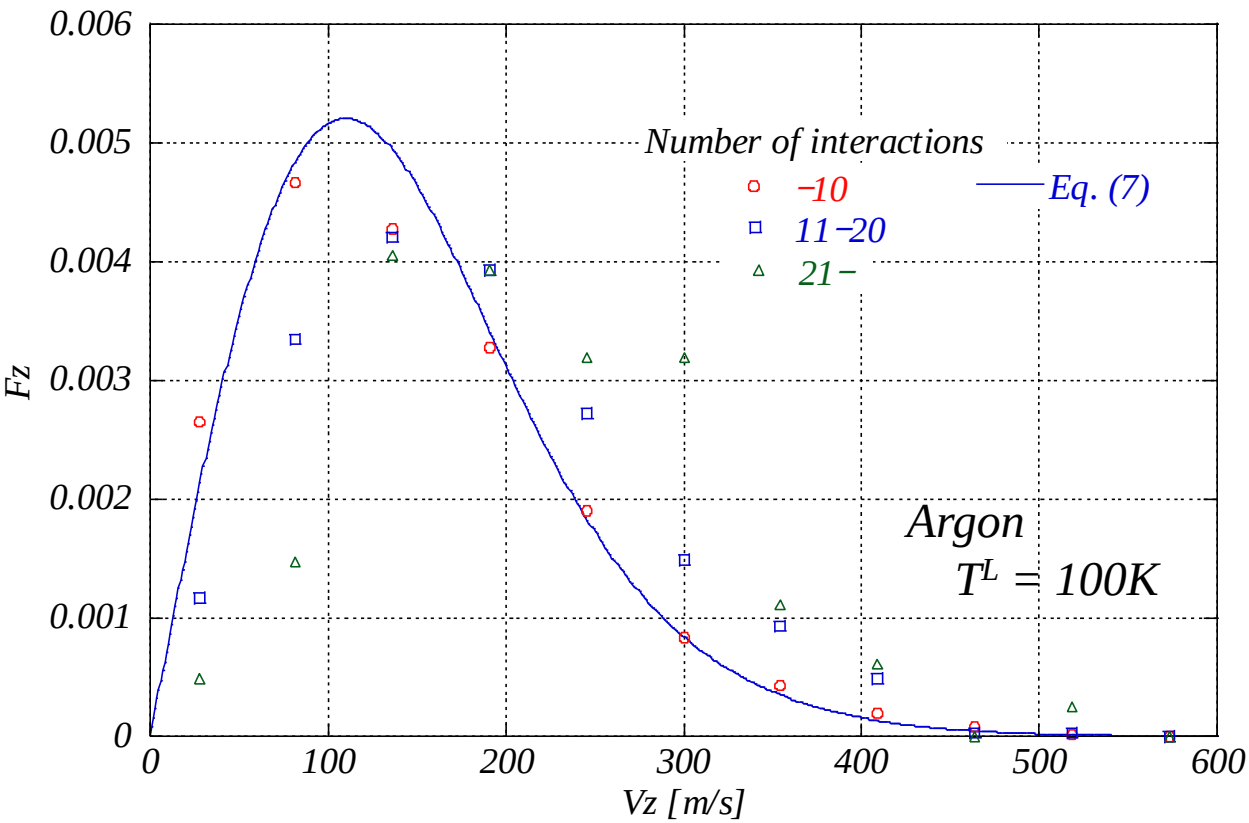

(b) Classification of reflecting molecules based on number of interactions (130K-100K)

Fig. 9 Velocity distribution of reflecting molecules on the condensing surface at 100 K (T_H=130 K). The velocity distribution (a) shows some shift to the larger velocity region compared to the equilibrium velocity distribution given by Eq. (7). The velocity distribution (b) shows the relation between the interaction number and their velocity distribution density.

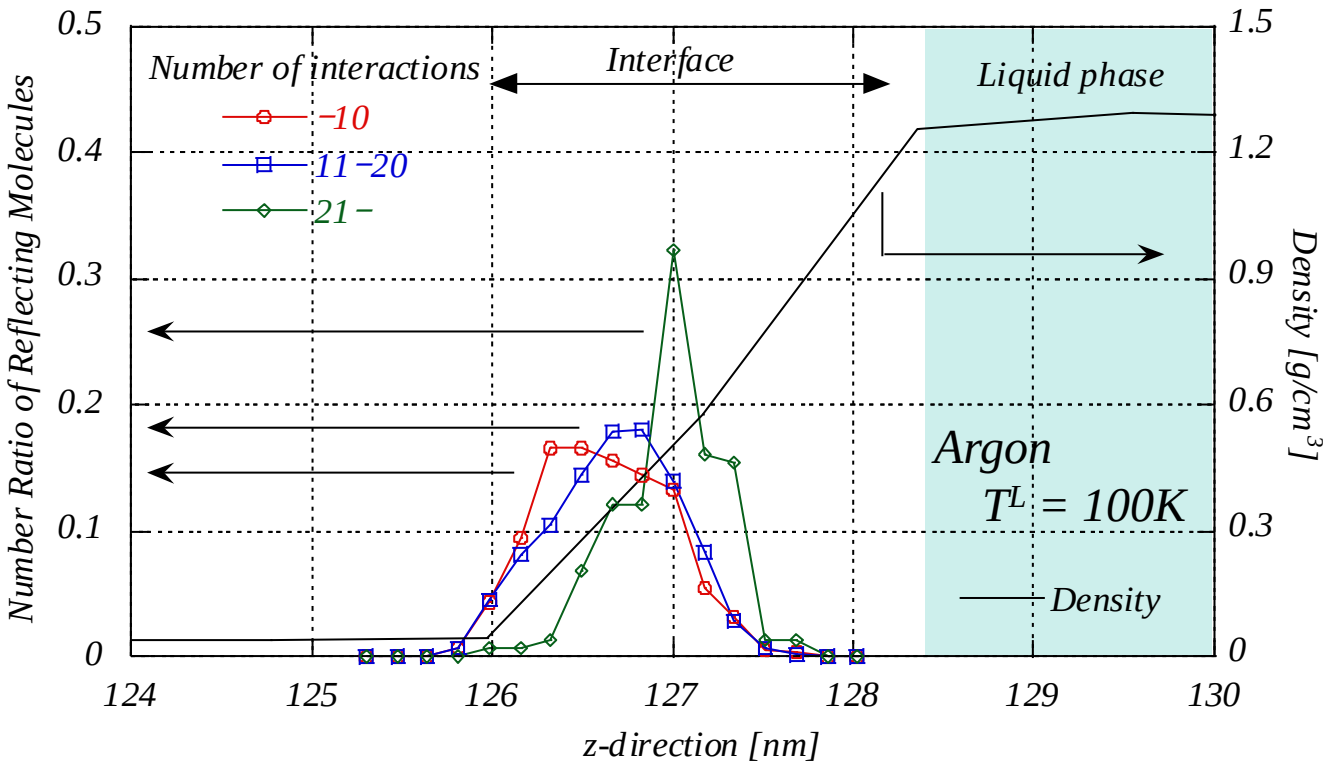

Fig. 10 Location of reflection in z direction within the interface region for the case of T^H = 130 K and T^L = 100 K.

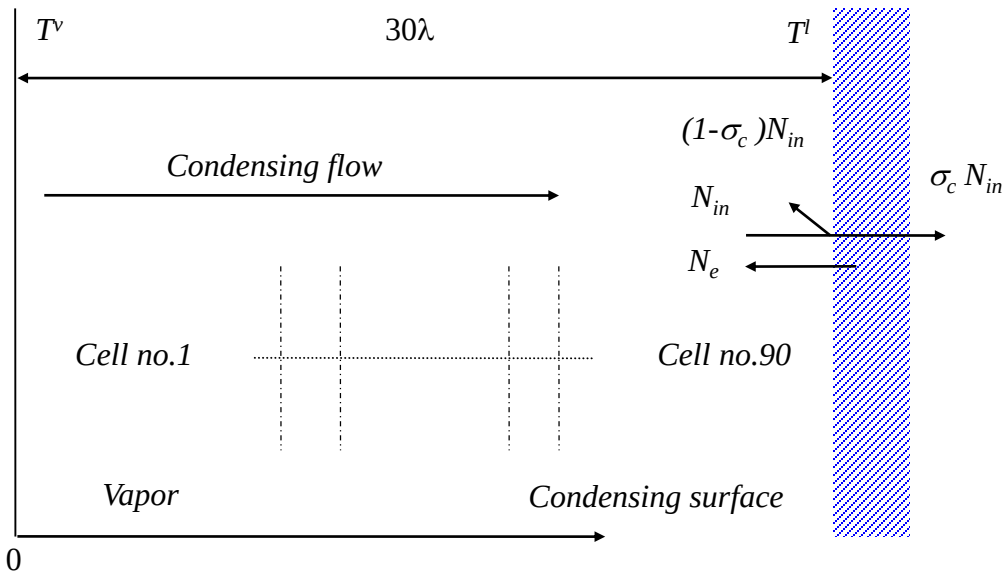

Fig. 11 Simulation system and boundary conditions for DSMC analysis

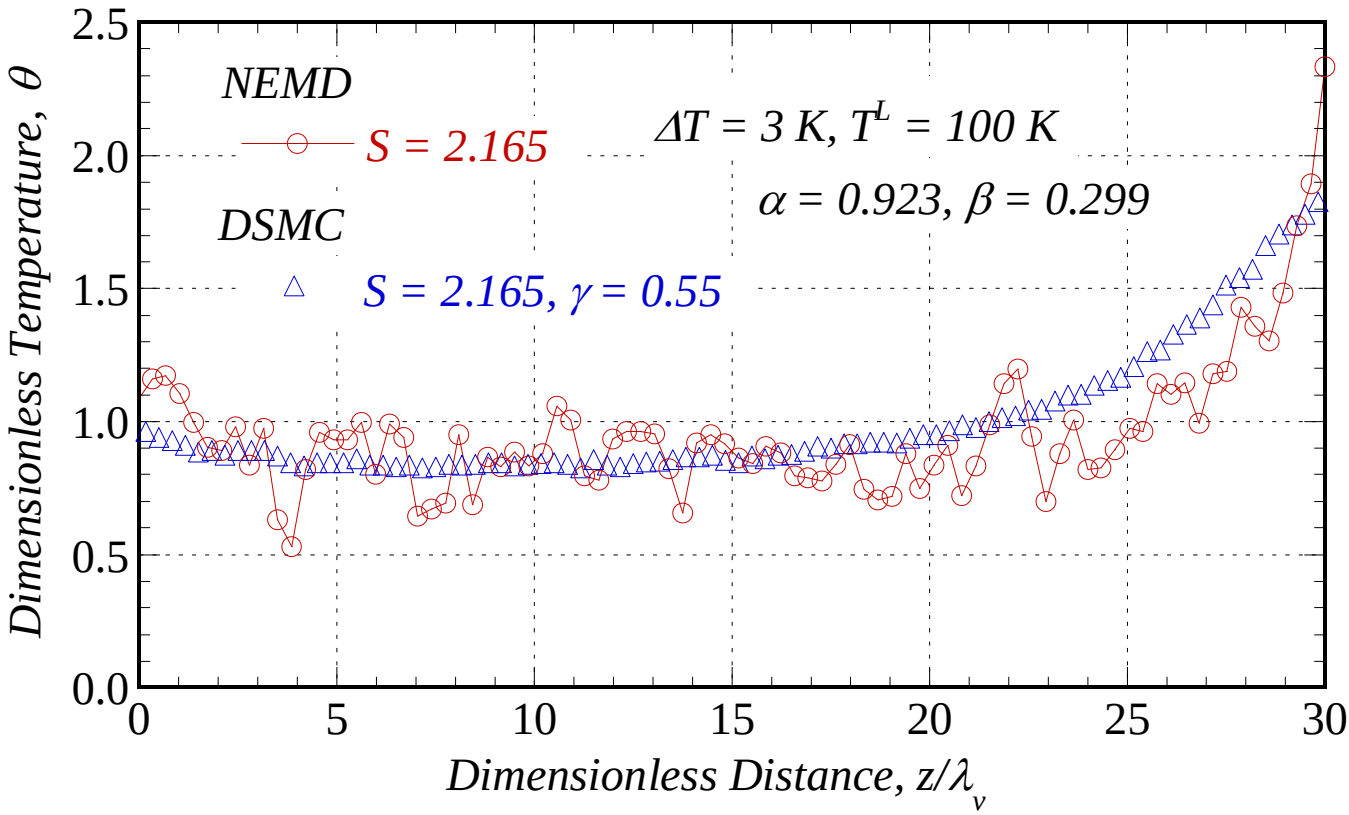

Fig. 12 Comparison of temperature profiles between NEMD and DSMC

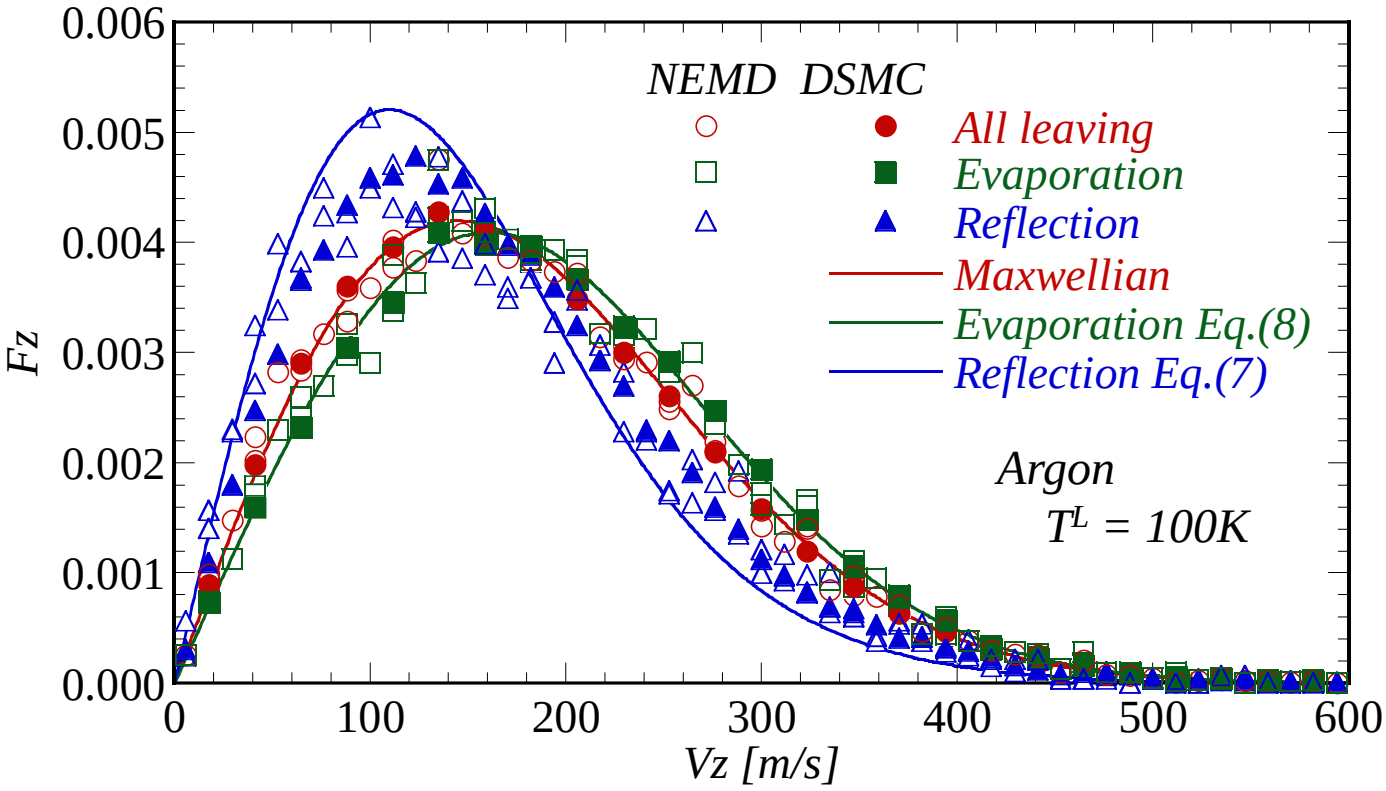

Fig. 13 Comparison of velocity distributions obtained by conducting NEMD simulations and DSMC analysis